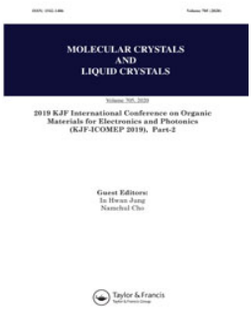

Molecular Crystals and Liquid Crystals

ISSN: 1542-1406 (Print) 1563-5287 (Online) Journal homepage: https://www.tandfonline.com/loi/gmcl20

Comparative study of phenyl-ester polymer-based organic solar cells with different solvents and additives

Hyunjung Jin, Um Kanta Aryal, Yeong-Soon Gal & Sung-Ho Jin

To cite this article: Hyunjung Jin, Um Kanta Aryal, Yeong-Soon Gal & Sung-Ho Jin (2020) Comparative study of phenyl-ester polymer-based organic solar cells with different solvents and additives, Molecular Crystals and Liquid Crystals, 705:1, 71-78, DOI: 10.1080/15421406.2020.1741826

To link to this article: https://doi.org/10.1080/15421406.2020.1741826

Published online: 18 Sep 2020.

MOLECULAR CRYSTALS AND LIQUID CRYSTALS
2020, VOL. 705, NO. 1, 71–78
https://doi.org/10.1080/15421406.2020.1741826

Comparative study of phenyl-ester polymer-based organic solar cells with different solvents and additives

Hyunjung Jin[a], Um Kanta Aryal[a], Yeong-Soon Gal[b], and Sung-Ho Jin[a]

[a]Department of Chemistry Education, Graduate Department of Chemical Materials, and Sustainable Utilization of Photovoltaic Energy Research Center, Pusan National University, Busan, Republic of Korea; [b]Polymer Chemistry Laboratory, College of Engineering, Kyungil University, Gyeongsan, Republic of Korea

ABSTRACT

Organic solar cells (OSCs) have been attracting strong research interest as a promising clean renewable energy source due to their beneficial characteristics such as lightweight, mechanical flexibility, low cost, and solution processability. Herein, phenyl ester-based donor polymer (Ph-Ester-BTF) and [6]-phenyl C71-butyric acid methyl ester ($PC_{71}BM$) acceptor was used as photoactive materials for the OSCs. With using Ph-Ester-BTF polymer as donor for OSCs, power conversion efficiency (PCE) was obtained as 2.68% for pristine chlorobenzene (CB) processed OSCs. Different solvents and additives were used for comparative study, wherein pristine CB yielded the better photovoltaic device performance of OSCs. Charge carrier mobility and film surface morphology was studied for further interpretation of the device performance.

KEYWORDS

charge transportation; organic solar cells; photovoltaic performance; processing solvents; surface morphology

1. Introduction

Organic solar cells (OSCs) have drawn great attention in both academia and industry due to their huge potential and apparent advantages of synthetic variability, easy fabrication, light weight, low cost, mechanical flexibility, large area roll to roll fabrication and the solution processability [1–4]. Bulk-heterojunction (BHJ) OSCs consists of polymer donor and acceptor blending thin layer sandwiched between cathode (low work function negative electrode) and anode (high work function positive electrode). Electron and hole transporting layers are used toward the cathode and anode for the more effectiveness in transportation and collection of respective charge carriers toward respective electrodes.

Mainly, for the improvement of the BHJ film morphology, device engineering with appropriate architecture, and insertion of the interfacial materials between different layers play key role for the better performance of OSCs [5–8]. Among them, nanoscale thin film morphology is one of the vital factor controlling recombination process in the BHJ photoactive composite [9,10]. The photoactive layer morphology can be tuned by

CONTACT Sung-Ho Jin shjin@pusan.ac.kr Department of Chemistry Education, Graduate Department of Chemical Materials, and Sustainable Utilization of Photovoltaic Energy Research Center, Pusan National University, Busan, 46241, Republic of Korea

proper processing methods like; selection of appropriate solvents, additives combination, solvent and thermal annealing, different thin film processing conditions etc [11–14]. Generally, the proper combination of the solvents like chlorobenzene (CB), dichlorobenzene (o-DCB), o-xylene, toluene with additives 1,8-diiodoctane (DIO), diphenyl ether (DPE), 1,8-octanedithiol (ODT) affects the size of fullerene domains by improving blends solubility for fine films [15–17]. Some cases the solvents without additives also found good film morphology for effective OSCs device performance due to proper alignment and good miscibility of donor and acceptor materials with processing solvents [18,19].

Herein, in order to study the influence of solvent and additives, we used our new synthesized donor, phenyl ester-based polymer (Ph-Ester-BTF) with [6]-phenyl C71 butyric acid methyl-ester (PC71BM) acceptor using different solvents; CB, o-DCB, toluene, o-xylene and co-solvents DPE and DIO. Among these pristine CB solvent processed OSCs yielded the best device performance as 2.68% as compare to remaining cases. While using additive DPE and DIO, slightly reduced the device performance. The varied concentration of donor:acceptor (D:A) ratio (1:1, 1:1.5 and 1:2) processed by pristine CB solvent were applied, wherein the D:A ratio (1:1 and 1:2) slightly decreased PCE to 1.97 and 2.56%, respectively. The photoactive film surface morphology and the transportation property for Ph-Ester-BTF based devices were analyzed further for supportive of the performance of Ph-Ester-BTF polymer based OSCs.

2. Experimental section

2.1. General information

Synthesis of Monomers and Polymer: Compound one was synthesized according to reported procedures [20] and confirmed by 1H NMR. Monomer A1 was purchased from the Sunatech (China).

2.2. Synthesis of materials

Synthesis of 1, 4- Benzenedicarboxylic acid, 2, 5- dibromo-, 1, 4- bis(2- hexyldecyl) ester (1): ^{1}H NMR (300 MH_Z, $CDCl_3$): δ (ppm) 7.99 (m, 2H), 4.24-4.25 (m, 4H), 1.76 (m, 2H), 1.26 (m, 48H), 0.86 (m, 12H).

Synthesis of 1, 3- Benzenedicarboxylic acid, 4, 6- di- 2- thienyl-, 1, 3- dihexyldecyl ester (2): Compound 1 (1 g, 1.28 mmol) and 2-tributylstannyl thiophene (0.92 g, 2.56 mmol) were dissolved in anhydrous toluene (15 mL) and purge with nitrogen for 15 min, then 25 mg of $(PdPPh_3)_4$ was added and refluxed for overnight. The reaction mixture was cooled to room temperature and the solvent was removed. Crude product was extracted with methylene chloride, washed with water, brine solution, and dried over anhydrous sodium sulfate. The resulted crude was purified by column chromatography on silica gel with hexane as an eluent to furnish colorless liquid (0.7 g, 70%). ^{1}H NMR (300 MH_Z, $CDCl_3$): δ (ppm) 7.78 (m, 2H), 7.36 (m, 2H), 7.07 (m, 4H), 4.05 (m, 4H), 1.47 (m, 2H), 1.23 (m, 48H), 0.87 (m, 12H). ^{13}C NMR (75 MH_Z, $CDCl_3$): δ (ppm) 168.27, 140.60, 134.09, 133.16, 131.78, 127.53, 126.77, 68.59, 37.08, 31.90, 30.94, 29.90, 26.66, 14.15.

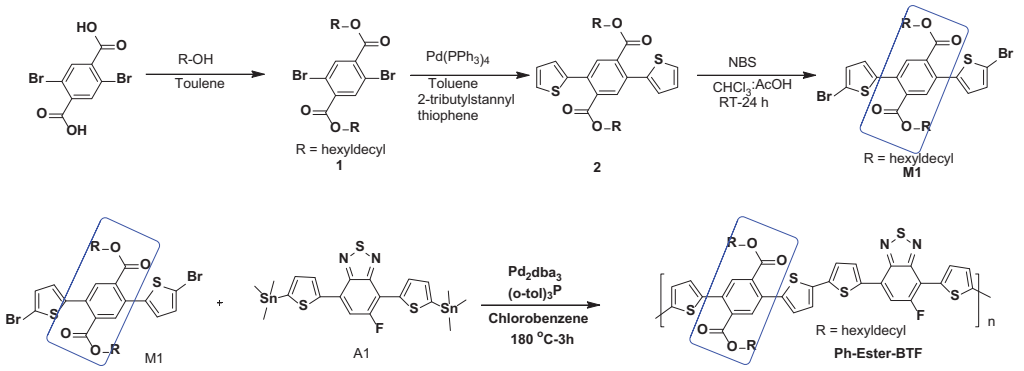

Scheme 1. Synthetic route for monomers and polymer.

Synthesis of 1, 4- benzenedicarboxylic acid, 2, 5- bis(5- bromo- 2- thienyl) -, 1, 4- dihexyldecyl ester (M1): Compound 2 (0.6 g, 0.76 mmol) was dissolved in chloroform (10 mL) and acetic acid (10 mL) and NBS (0.263 g, 1.53 mmol) was added and stir it at room temperature for overnight. Crude product was extracted with methylene chloride, washed with water, brine solution, and dried over anhydrous sodium sulfate. The resulted crude was purified by column chromatography on silica gel with hexane as an eluent to furnish colorless liquid (0.5 g, 70%). ^{1}H NMR (300 MH_Z, $CDCl_3$): δ (ppm) 7.74 (m, 2H), 7.01 (m, 2H), 6.83 (m, 2H), 4.07 (m, 4H), 1.50 (m, 2H), 1.23 (48H), 0.87 (m, 12H).^{13}C NMR (75 MH_Z, $CDCl_3$): δ (ppm)167.67, 141.90, 133.98, 132.73, 131.98, 130.37, 127.21, 126.74, 113.44, 68.85, 37.13, 31.87, 31.87, 29.62, 26.71, 22.73, 14.18.

Synthesis of polymer: To a 10 mL microwave tube, compound M1 (0.275 mmol), and (A1) (0.275 mmol) and anhydrous chlorobenzene (3 mL) were added and purged with nitrogen for 20 min, then Pd_2 $(dba)_3$ (2 mol %), and $(o$- $tol)_3P$ (16 mol %) were added. The reaction mixture was purged with nitrogen for 15 min. The microwave tube was placed into the reactor and heated to 180 °C for 3 hrs. After cooling to room temperature reaction mixture was poured into methanol to obtain precipitate. The resulted precipitate was purified by soxhlet extraction method using methanol, hexane, acetone, and chloroform. The chloroform fraction was evaporated to get polymer (60%) (Scheme 1). M_n=21713 g/mol, PDI = 1.59. Elemental Analysis: Anal. Calcd for C62H79FN2O4S5: Cal: C, 67.97; H, 7.27; N, 2.56. Found, C, 67.06; H, 6.99; N, 2.63.

2.3. Device fabrication and measurements

Device fabrication: Indium tin oxide (ITO)-coated glass substrates were taken and by using sonication process, they were cleaned with deionized water, acetone and isopropyl alcohol sequentially. Then the substrates dried with N_2 flow. The dried substrates were processed for plasma treatment in UV-ozone for 15 min. The cleaned samples were used for spin coating of ZnO layer at 2000 rpm for 40 s (40 nm thickness). The samples were kept for annealing at 150 °C for 20 min on a hot plate. Then the samples were transferred to glove box. The photoactive layer blend, Ph-Ester-BTF:PC_{71}BM varying concentration and solvents was prepared and spin coated above the ZnO layer for optimized thickness of 100 nm. Finally, MoO_3 of 7 nm and Ag of 100 nm was thermally evaporated sequentially using a shadow mask, adjusting a device active area of 0.11 cm^2.

Measurement and characterization of OSCs: For the measurement of photovoltaic performance of OSCs, we used calibrated air mass 1.5 G solar simulator (Oriel Sol3A Class AAA solar simulator, models 94043 A, Newport Stratford, Inc., USA) with a light intensity of 100 mW/cm^2 adjusted using a standard PV reference cell (2 cm × 2 cm monocrystalline silicon solar cell, calibrated at NREL, Golden, CO) and a computer controlled Keithley 2400 (Keithley Instruments, Inc. USA) source measure unit solar simulator (oriel Sol3A Class AAA solar simulator, models 940443 A) with a computer controlled Keithley-2400 source measure unit. Using Oriel IQE-200 with a 250 W quartz tungsten halogen lamp the incident photon to current efficiency (IPCE) was analyzed. The thickness of the different layers of the device were determined by using KLA tencor Alpha-step IQ surface profile-ometer with an accuracy of ±1 nm. The hole and electron mobility were determined using hole only and electron only device's current density-voltage (*J-V*) characteristics and fitting by the space charge limited current (SCLC) method. The mobility was found by fitting the dark *J-V* curve into the SCLC model, based on Mott-Gurney law. For analyzing surface morphology, atomic force microscopy (AFM) images were captured using a XE-100 AFM (Park system corp., Korea).

3. Results and discussion

The measured UV-vis absorption spectra of the polymer in solution and film state are depicted in Figure 1a. The solution and film both state exhibited similar absorption peak, in which especially the broad absorption profiles were exhibited in range of 300-700 nm. That indicates that the polymer could effectively absorb the solar flux for contribution of photocurrent generation. By using gel permeation chromatography (GPC), the molecular weight of the polymer was estimated as (Mn = 21713 Da: PDI = 1.59). Further, the onset of decomposition temperature (T_d, corresponding to 5% weight loss) was calculated as 370 °C (Figure 1b), that consists sufficient thermal stability of the polymer for the applications of optoelectronics. The highest occupied molecular orbitals (HOMO) level and lowest unoccupied molecular orbitals (LUMO) level by using cyclic voltammetry (CV) were determined as −5.40 and −3.76 eV, respectively as illustrated CV plots in Figure 1c. Moreover, density functional theory (DFT) simulations for the Ph-Ester-BTF polymer was conducted for better understand the electronic properties in details. The obtained values of HOMO and LUMO are −4.47 and −2.30 eV, respectively, depicted in Figure 1d. There is good alignment between the experimental and simulation results.

The molecular structure of the photoactive materials (Ph-Ester-BTF donor polymer and PC71BM acceptor) which are used in this study are as shown in Figure 2a. The device configuration of ITO/ZnO/Ph-Ester-BTF:$PC_{71}BM$/MoO_3/Ag applied for OSCs device is illustrated in Figure 2b. First of all, we used different pristine solvents CB, o-DCB, o-xylene and toluene. Among these, the best device performance was with CB solvent, achieved as PCE of 2.68% (with open circuit voltage (V_{OC}) of 0.94 V, short circuit current density (J_{SC}) of 6.63 mA/cm^2 and fill factor (FF) of 42.97%). While using additives DPE and DIO with CB solvent, suddenly the device PCE decreased to 2.11% and 1.94%. The detailed photovoltaic parameters table with different solvents and additives are summarized in Table 1. Further we varied the D:A ratio of 1:1 and 1:2,

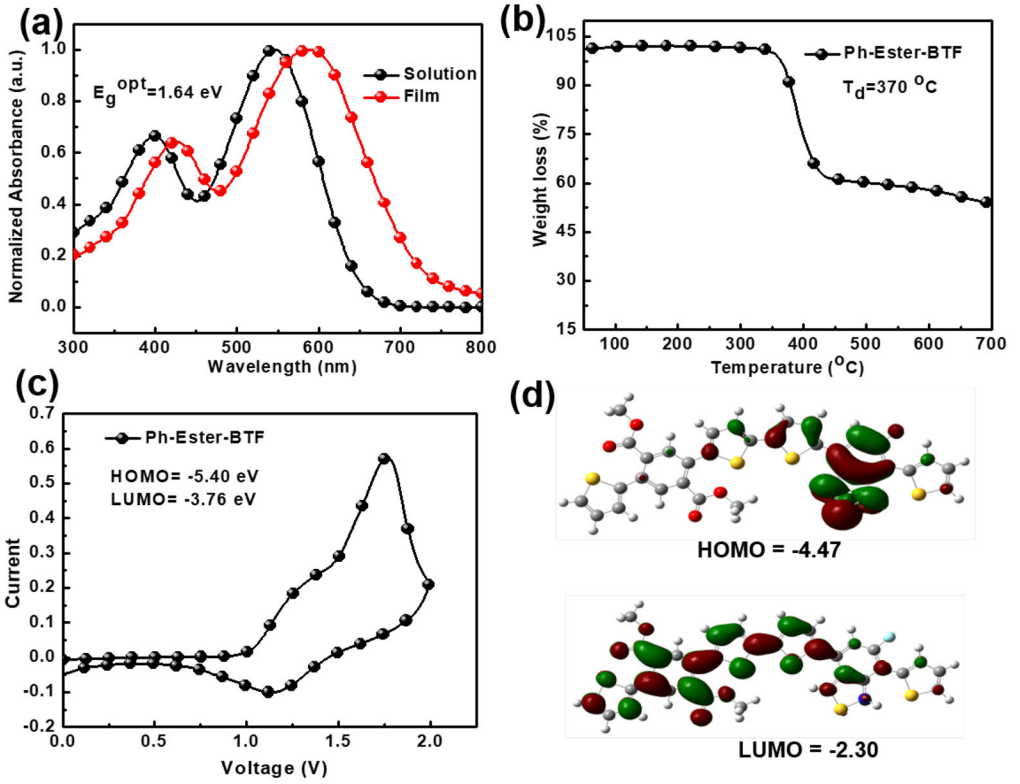

Figure 1. (a) UV-vis absorption spectra in solution and film state (b) TGA plot (c) CV measurement and (d) DFT HOMO/LUMO of Ph-Ester-BTF polymer.

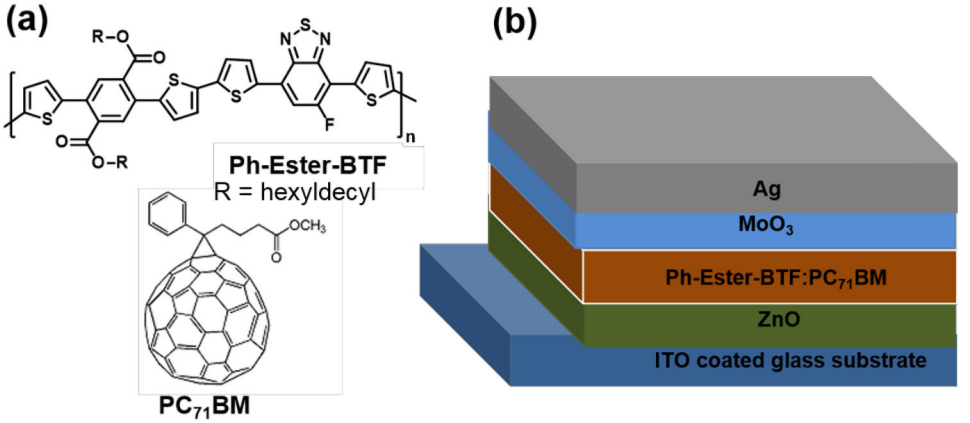

Figure 2. (a) Molecular structure of donor, acceptor. (b) Device configuration of OSCs.

obtained PCE of 1.97% and 2.56%, respectively. The pristine CB solvent devices with D:A ratio of 1:1.5 achieved the best conditions (PCE of 2.68%) in this study. The detailed photovoltaic parameters with variation of D:A ratio is tabulated in Table 2, and the respective *J-V* and external quantum efficiency (EQE) curves are shown in Figure 3a

Table 1. Photovoltaic performance of Ph-Ester-BTF:$PC_{71}BM$ based OSCs processed with different solvents and additives.

Devices	Solvents: Additives	V_{OC} (V)	J_{SC} (mA/cm^2)	FF (%)	PCE (%)
1	CB	0.94	6.63	42.97	2.68
2	CB:DPE	0.93	5.18	43.66	2.11
3	CB:DIO	0.92	4.95	42.43	1.94
4	o-DCB	0.89	5.94	41.13	2.18
5	o-xylene	0.87	5.81	40.64	2.06
6	o-xylene:DPE	0.84	5.93	33.98	1.71
7	Toluene	0.92	4.95	42.43	1.94

Table 2. Photovoltaic performance of Ph-Ester-BTF:$PC_{71}BM$ based OSCs processed with pristine CB solvent varying donor:acceptor (D:A) ratio.

Devices	D:A (ratio)	V_{OC} (V)	J_{SC} (mA/cm^2)	FF (%)	PCE (%)	Integrated J_{SC} (mA/cm^2)
1	1:1	0.92	4.92	43.23	1.97	4.81
2	1:1.5	0.94	6.63	42.97	2.68	6.56
3	1:2	0.93	6.68	41.00	2.56	6.62

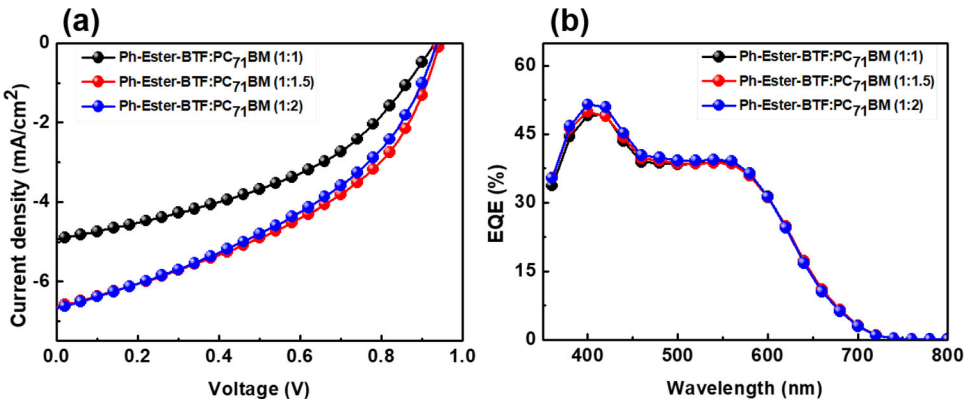

Figure 3. (a) *J–V* curve and (b) EQE spectra of Ph-Ester-BTF:$PC_{71}BM$-based OSCs.

and b, respectively. The EQE spectra of OSCs performed similar EQE spectra over the 360-800 nm wavelength and improved photoresponse peaks in 360-600 nm wavelength (Figure 2b). The integrated J_{SC} values determined from EQE curves were as 4.81, 6.56 and 6.62 mA/cm^2 for the devices of ratio 1:1, 1:1.5 and 1:2, respectively. The integrated J_{SC} values are well matched with the J_{SC} values obtained from *J-V* measurements of solar simulator, accordance with the performance of OSCs.

The surface morphology of photoactive layer with polymer was analyzed via measuring tapping-mode atomic force microscopy (AFM). We measured pristine blend with CB and blend with CB:DPE as illustrated in Figure 4. The root mean square (RMS) roughness values for the pristine blend was measured as 2.50 nm. While adding DPE additive in CB solvent, the RMS value slightly increased to 3.14 nm. The rougher surface with additive could affect for compatibility of photoactive layer and the charge transporting layers, which distracts for charge transportation and collection toward respective electrodes. Therefore, the pristine blend maintained better FF and J_{SC}, resulting the good film morphology for effectively charge transportation and

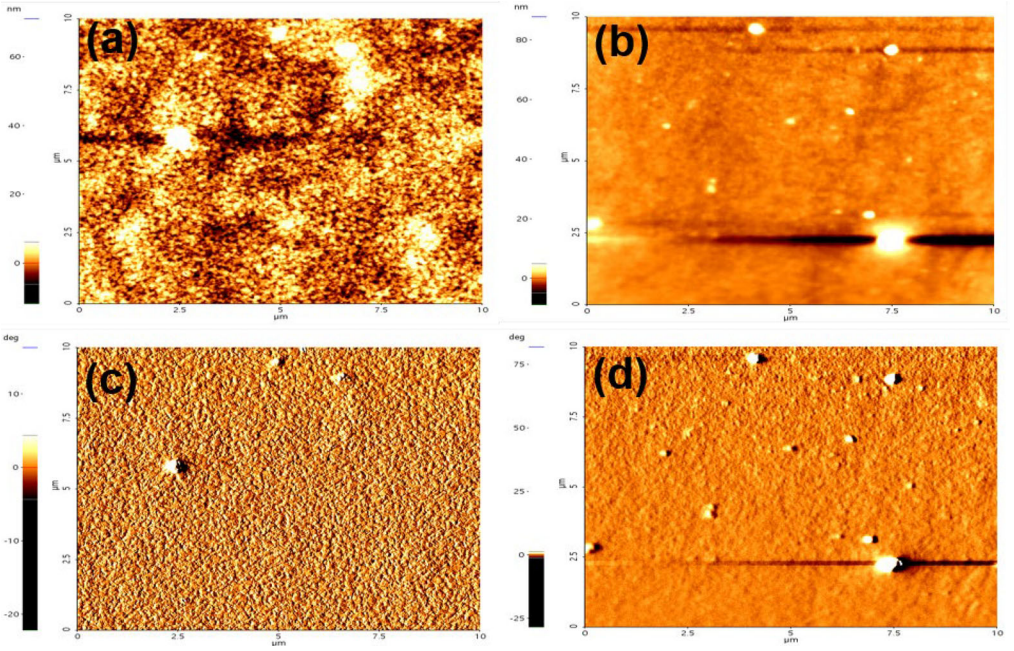

Figure 4. AFM images of Ph-Ester-BTF:$PC_{71}BM$ films processed with pristine CB solvent and CB with DPE (a, b) height images and (c, d) phase images, respectively.

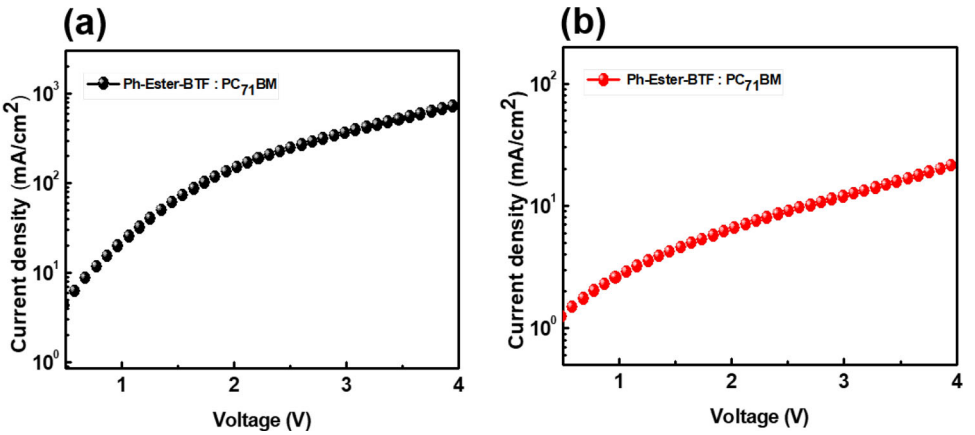

Figure 5. *J*–*V* curves of (a) hole-only devices for hole mobility measurement and (b) electron-only devices for electron mobility measurement.

enhancement of overall photovoltaic performance of the OSCs on comparing with additive based blend devices.

Charge transportation property of OSCs with photoactive materials applying our best conditions was conducted with the hole only device of architecture ITO/PEDOT:PSS/Ph-Ester-BTF:PC71BM/MoO3/Al and electron only device of architecture ITO/ZnO/Ph-Ester-BTF:PC71BM/LiF/Ag. The hole and electron mobility were calculated by applying the SCLC model based on the Mott-Gurney laws equation, $J = (9/8)\ \varepsilon r\ \varepsilon_0\ \mu\ (V2/L3)$, where εr is the dielectric constant ($\varepsilon r = 3$), ε_0 the permittivity of free space, μ the charge

carrier mobility, V the voltage drop across the device and L the thickness of the photoactive layer [20]. The measured dark *J-V* curve for hole and electron only device illustrated in Figure 5a and b, respectively. The hole mobility was calculated as 1.77×10^{-4} cm^2/V s and the electron mobility was estimated as 8.21×10^{-5} cm^2/V s. These balancing carrier mobility values further supportive for charge transportation and collection effectively toward respective electrode sides as using Ph-Ester-BTF polymer as donor in photovoltaic devices

4. Conclusion

In summary, we successfully applied the new designed phenyl ester-based (Ph-Ester-BTF) polymer as donor for OSCs. In this study, using different solvents and co-solvents, pristine CB processed conditions optimized the best photovoltaic performance of OSCs. For the pristine CB processed devices, the D:A ratio was varied and D:A (1:1.5) obtained the PCE of 2.68%. Adding additives, slightly changed the morphological texture of the photoactive layer and deducted the Ph-Ester-BTF based OSCs performance. The balancing charge carriers mobility further supportive for the extraction and transportation of the charge carrier toward the respective electrodes effectively and exhibiting the good performance of Ph-Ester-BTF polymer based OSCs.

Funding

This work was supported by a grant fund from the National Research Foundation (NRF) (NRF-2018R1A5A1025594) by the Ministry of Science, ICT of Korea.

References

[1] G. Li, R. Zhu, and Y. Yang, *Nature Photon.* **6** (3), 153 (2012). doi:10.1038/nphoton.2012.11
[2] W. Cao, and J. Xue, *Energy Environ. Sci.* **7** (7), 2123 (2014). doi:10.1039/c4ee00260a
[3] G. Yu *et al.*, *Science* **270** (5243), 1789 (1995). doi:10.1126/science.270.5243.1789
[4] Y.-W. Su, S.-C. Lan, and K.-H. Wei, *Mater. Today* **15** (12), 554 (2012). doi:10.1016/S1369-7021(13)70013-0
[5] W. Ma *et al.*, *Adv. Energy Mater.* **5** (23), 1501400 (2015). doi:10.1002/aenm.201501400
[6] C.-C. Chen *et al.*, *Adv. Mater. Weinheim.* **26** (32), 5670 (2014). doi:10.1002/adma.201402072
[7] X. Yang *et al.*, *ACS Appl. Mater. Interfaces* **9** (1), 618 (2017). doi:10.1021/acsami.6b11063
[8] U. K. Aryal *et al.*, *Org. Electron.* **63**, 222 (2018). doi:10.1016/j.orgel.2018.09.034
[9] S. Albrecht *et al.*, *J. Am. Chem. Soc.* **134** (36), 14932 (2012). doi:10.1021/ja305039j
[10] D. Credgington *et al.*, *Adv. Mater. Weinheim.* **24** (16), 2135 (2012). doi:10.1002/adma.201104738
[11] X. Liu *et al.*, *J. Mater. Chem. A* **6** (2), 395 (2018). doi:10.1039/C7TA10136H
[12] C. Liu *et al.*, *Nanoscale* **6** (23), 14297 (2014). doi:10.1039/C4NR04958F
[13] G. L. Schulz *et al.*, *Beilstein J. Nanotechnol.* **4**, 680 (2013). doi:10.3762/bjnano.4.77
[14] U. K. Aryal *et al.*, *ACS Appl. Energy Mater.* **2** (6), 4159 (2019).
[15] A. Foertig *et al.*, *Adv. Funct. Mater.* **24** (9), 1306 (2014). doi:10.1002/adfm.201302134
[16] L. Li *et al.*, *ACS Appl. Mater. Interfaces* **7** (38), 21495 (2015). doi:10.1021/acsami.5b06691
[17] U. K. Aryal *et al.*, *Macromol. Res.* **26** (13), 1276 (2018). doi:10.1007/s13233-019-7075-7
[18] K. Kranthiraja *et al.*, *Adv. Mater.* **29** (23), 1700183 (2017). doi:10.1002/adma.201700183
[19] Q. An *et al.*, *Science Bull.* **64** (8), 504 (2019). doi:10.1016/j.scib.2019.03.024
[20] P. N. Murgatroyd, *J. Phys. D: Appl. Phys.* **3** (2), 151 (1970). doi:10.1088/0022-3727/3/2/308